Empirical Assessment of Geometric Accuracy of Underwater Lidar in Tropical Shallow Waters

Mentari K. Azzahra [1], Fickrie Muhammad [2], Arnadi Murtiyoso [3], Annette Scheider [4], Harald Sternberg [4], Gabriella Alodia [2]

[1] Institut Teknologi Bandung, Faculty of Earth Sciences and Technology, Geodesy and Geomatics Engineering Postgraduate Programme, Bandung, Indonesia - 25125014@mahasiswa.itb.ac.id
[2] Institut Teknologi Bandung, Faculty of Earth Sciences and Technology, Hydrography Research Group, Bandung, Indonesia – (fickrie, gabriella.alodia)@itb.ac.id
[3] Université de Strasbourg, CNRS, INSA Strasbourg, ICube Laboratory UMR 7357, Photogrammetry and Geomatics Group, Strasbourg, France - arnadi.murtiyoso@insa-strasbourg.fr
[4] HafenCity University Hamburg, Department of Hydrography and Geodesy, Hamburg, Germany – (annette.scheider, harald.sternberg)@hcu-hamburg.de

Keywords: Underwater Lidar, Laser Scanners, Hydrography, Photogrammetry.

Abstract

This study empirically evaluates the geometric accuracy of point cloud data acquired using an underwater lidar (ULi) system in a tropical shallow water environment. The field test was conducted in the tropical waters of the Seribu Islands, Indonesia, characterised by relatively low turbidity. Terrestrial laser scanning (TLS) and close-range photogrammetry were employed as independent reference datasets. Geometric discrepancies between datasets were quantified using the multiscale model-to-model cloud comparison (M3C2) algorithm, and errors were statistically characterised using the median and median absolute deviation (MAD) to ensure robustness under non-normal distributions. The results indicate that the error of ULi relative to TLS is 0.008 ± 0.012 m, while the error relative to photogrammetry is 0.006 ± 0.013 m. In comparison, the discrepancy between photogrammetry and TLS is smaller, at 0.002 ± 0.004 m. Dimensional analysis of an acoustic Doppler current profiler (ADCP) frame further shows that ULi agrees with TLS and photogrammetry within the millimetre to centimetre range (0.000–0.015 m). Larger deviations in specific segments are attributed to local effects, including edge-related artefacts. Overall, the results demonstrate that ULi provides reliable geometric measurements in shallow-water conditions with low turbidity. Despite slightly lower accuracy compared to terrestrial methods, the system shows potential for underwater mapping applications, particularly in shallow water environments.

1. Introduction

The growing development of underwater infrastructure has increased the demand for underwater inspection and maintenance operations (Sørensen et al., 2025). The effectiveness of these activities depends on accurate measurements (Koziel et al., 2021). Current underwater surveying technologies rely primarily on cameras and sonar. However, underwater imaging is affected by multiple factors, including image blurring, reduced contrast, turbidity, and non-uniform light attenuation caused by the seawater medium. In parallel, sonar performance is limited by suspended solids, air bubbles, and interference from nearby acoustic sources. Moreover, the predominantly downward-facing acquisition geometry leads to reduced point density along the sides of underwater structures (Rho et al., 2025; Sørensen et al., 2025; Yang et al., 2019). To address the need for detailed underwater surveys, light detection and ranging or lidar systems have been developed and gradually commercialised for underwater applications (Fraunhofer Institute for Physical Measurement Techniques IPM, 2024; Kraken Robotics, 2025; Voyis, 2021).

Lidar systems have been widely applied across various spatial domains (Hillman et al., 2021; Li et al., 2022; Rashdi et al., 2024). In recent years, studies on the range precision and spatial resolution of underwater lidar (ULi) systems have primarily been conducted under controlled laboratory conditions with static configurations (Heffner et al., 2025; Walter et al., 2025). However, assessments of their geometric accuracy in real-world environments remain limited. This gap is significant, as the accuracy of laser scanner-derived point clouds is essential for capturing detailed environmental information and enabling efficient data use by engineers and scientists (Rashdi et al., 2024). Because geometric accuracy is affected by multiple systematic error sources, including environmental conditions and the accuracy of the navigation solution, its impact on point cloud quality is difficult to predict (Bobrowski et al., 2023; Rashdi et al., 2024; Walter et al., 2025). Therefore, robust ground-truth data are crucial for evaluating and constraining the geometric accuracy of ULi systems.

The performance of underwater lidar is strongly influenced by water turbidity, as signal penetration depth decreases with increasing turbidity (Saylam et al., 2017; Zimmerman et al., 2013). Under controlled laboratory conditions with a turbidity level of 0 NTU, Heffner et al. (2025) reported a range precision of 1.95 mm from repeated measurements on a metal plate, while Walter et al. (2025) showed a spatial resolution of up to 2.95 mm from Böhler star measurements for scanning distances of up to 8.03 m. In the same study, field experiments involving dynamic, vessel-based operations were conducted in the Elbe River. Due to the high turbidity, which exceeds 6 NTU, the Secchi depth was less than 1.1 m. For that reason, it was not possible to acquire scan data of any structure.

To address this research gap, we conducted an experiment to assess the performance of an ULi system in a real-world setting. The ULi system, developed by Fraunhofer IPM, was tested in the tropical waters of the Seribu Islands, Indonesia, by mapping a geometrically constrained object. The resulting point clouds were evaluated using cloud-to-cloud comparisons against ground-truth datasets obtained from terrestrial laser scanning (TLS) and photogrammetric mapping of the same object, thereby establishing a new reference for ULi performance in clear, shallow-water environments.

2. Data and Methods

2.1 Field data acquisition

A stainless-steel frame of an acoustic Doppler current profiler (ADCP) with known dimensions was selected as the measurement target due to its structural rigidity and reflectivity. Although highly reflective materials can be challenging to scan with laser scanning instruments, the frame has a relatively matte surface, which reduces potential issues during data acquisition (Figure 2b). According to Chen et al. (2020) and Werner et al. (2023), ULi systems operate based on the pulsed time-of-flight (ToF) principle, measuring travel time between pulse emission and the detection of the reflected signal. Lower system errors are typically observed for highly reflective materials, such as metals, making the ADCP frame well-suited for this experiment.

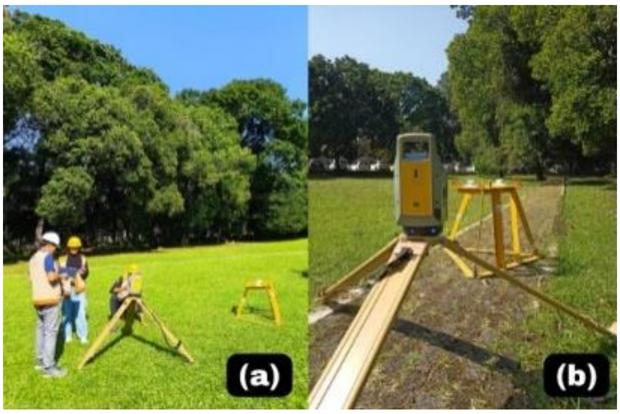

Figure 1. (a) Ground-truth data acquisition; (b) TLS setup during the measurement of the ADCP frame.

Figure 2. (a) ULi mounted on a fisherman’s vessel; (b) a dimensionally constrained ADCP frame used as a mapping target (c) ULi system; (d) GNSS receiver for positioning.

Ground-truth measurements using both TLS and photogrammetric methods were carried out in an open field at Institut Teknologi Bandung (Figure 1). The site is constrained by three semi-permanent benchmarks with known geographic and projected coordinates, ensuring strong geometric control for the terrestrial measurements. Several control points were installed on the frame and measured using a total station employing the intersection methods, providing constraints for both the TLS and photogrammetric point clouds during processing.

TLS data acquisition was conducted from four stations to ensure complete coverage of the ADCP frame. The resulting datasets were subsequently merged and georeferenced using Trimble Business Centre software. Pairwise registration was applied to align point clouds from different stations, followed by georeferencing based on the measured control point coordinates. Meanwhile, photogrammetric data were acquired by systematically capturing images around the ADCP frame to ensure full coverage and sufficient overlap. The images were then processed into point clouds using Agisoft Metashape software.

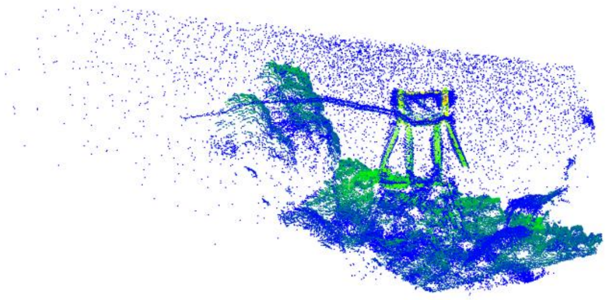

Figure 3. ULi point cloud acquired along a single survey line, showing the ADCP frame and its surrounding environment before segmentation.

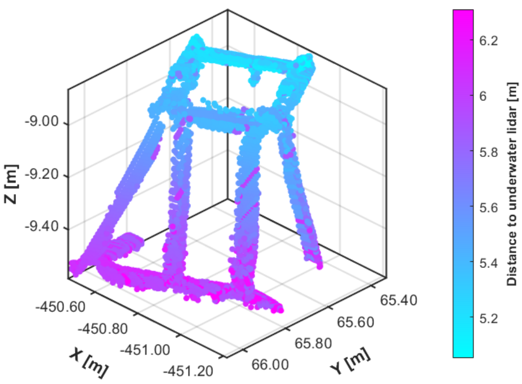

Figure 4. The acquisition distance to the ADCP frame in local coordinates.

Point clouds data	Instrument	Number of points	Mean Surface Density
ULi	Fraunhofer IPM Underwater Lidar	6,549	18,687
TLS	Trimble X7 3D Lasser Scanners	1,253,707	1,130,294
Photogrammetry	Nikon Z50	384,528	480,127

Table 1. Datasets used in this study

While the ground-truth measurements were conducted in a controlled environment, the field survey was carried out in the shallow waters of the Seribu Islands, where the ADCP frame was submerged and scanned kinematically using the ULi system. The study area was selected for its high water clarity, with visibility ranging from 9 to 12 m, as indicated by Secchi disk measurements. The ULi system was side-mounted on a 12-mlong wooden vessel, with positioning derived from post-processed global navigation satellite system–inertial navigation system (GNSS–INS), as presented in Figure 2. The dataset used in this study was limited to a single survey line, yielding point clouds of the ADCP frame and its surrounding environment at distances ranging from 5 to 6 m (Figures 3 and 4).

The datasets acquired during the field surveys are summarised in Table 1.

2.2 M3C2 distance calculation

The geometric accuracy of the ULi data was assessed by computing model-to-model cloud comparison (M3C2) distances between the ULi point cloud and reference point clouds derived from TLS and photogrammetry, using CloudCompare. According to Lague et al. (2013), the M3C2 algorithm is designed to provide accurate orthogonal distance measurements between two point clouds without requiring meshing or gridding. It is also robust to missing data and variations in point density between datasets.

Following the computation of M3C2 distances, the statistical distribution of the distances was evaluated using skewness and kurtosis to assess normality. Skewness is a measure of the asymmetry of a distribution, where a value of zero indicates a normal distribution (Iacobucci et al., 2025; Kim, 2013). It is expressed in Equation 1:

$$Skewness = \frac{\sum (x_i - \bar{x})^3}{n\sigma^3} \tag{1}$$

where x_i represents the individual M3C2 distance value, $\bar{x}$ is the mean M3C2 distance, and σ is the standard deviation, and n is the number of observations.

Kurtosis describes the peakedness and tail behaviour of a distribution. In this study, excess kurtosis is considered, which is obtained by subtracting 3 from the kurtosis value. A value of zero indicates a normal distribution (Iacobucci et al., 2025; Kim, 2013). It is defined in Equation 2:

$$Kurtosis = \frac{\sum (x_i - \bar{x})^4}{n\sigma^4} \tag{2}$$

2.3 Error analysis

Following the computation of M3C2 distances and the distribution analysis, the resulting values were analysed to obtain statistical parameters such as the mean (μ), standard deviation (σ), median (m), and median absolute deviation (MAD).

The measurement error of the ULi was evaluated based on the distribution of the M3C2 distance values. In the presence of outliers that lead to non-normal distributions, a robust nonparametric approach is required. In such cases, the median and the MAD are used as robust measures instead of the mean and standard deviation, respectively (Toschi et al., 2015).

Accordingly, the error (ε) is expressed in Equation 3, and the MAD is defined in Equation 4:

$$\varepsilon = |m| \pm MAD \tag{3}$$

$$MAD = m(|x_i - m(x)|) \tag{4}$$

in which x_i represents the individual M3C2 distance value, $m(x)$ is the median of the dataset, and $|x_i - m(x)|$ denotes the absolute deviation from the median.

2.4 ADCP frame dimension comparison

The dimensions of the ADCP frame were evaluated using point clouds generated from ULi, TLS, and photogrammetry. Manual digitisation in CloudCompare was performed to extract geometric features for dimensional comparison.

3. Results

3.1 Control point coordinates and point cloud datasets

The control point coordinates obtained using the intersection method were used to transform all point cloud datasets into a common reference frame, as shown in Figure 5. All datasets were subsequently segmented manually using CloudCompare software to obtain a representative 3D model of the ADCP frame.

3.2 M3C2 distance calculation results

The results of the M3C2 distance calculation are shown in Figure 6. Descriptive statistics of the M3C2 distance values are presented in Table 2, while skewness and kurtosis values shown in Table 3.

Dataset Comparison	μ	m	σ	MAD
ULi–TLS	-0.007	-0.008	0.023	0.012
ULi–Photogrammetry	-0.003	-0.006	0.022	0.013
Photogrammetry–TLS	-0.002	-0.002	0.008	0.004

Table 2. Descriptive statistics of M3C2 distance values for all dataset comparisons, including mean (μ), median (m), standard deviation (σ), and MAD in metres.

The M3C2 algorithm computes distances based on local neighbourhoods defined along the normal surface, where subsets of points from both the reference and compared point clouds are projected on the cylinder axis. As a result, reliable distance estimation depends on the availability of sufficient neighbouring points within the defined cylindrical volume for both datasets (Lague et al., 2013).

M3C2 distances were computed using TLS as the reference dataset for comparisons with ULi and photogrammetry. An additional comparison was performed between ULi and photogrammetry using photogrammetry as the reference.

As shown in Figure 6, the M3C2 distance values range from −8 cm to +8 cm. Positive values indicate that the compared point cloud is located above the reference surface along the normal direction, whereas negative values indicate that it is located below the reference.

Based on Table 3, the skewness values for all M3C2 distance comparisons are positive and close to zero, with the photogrammetry–TLS comparison showing the lowest value (0.211). This indicates that the distributions are generally normal with only slight positive skewness.

Dataset Comparison	Skewness	Kurtosis	Excess Kurtosis
ULi–TLS	0.247	3.223	0.223
ULi–Photogrammetry	0.363	3.316	0.316
Photogrammetry–TLS	0.211	7.368	4.368

Table 3. Skewness and kurtosis of M3C2 distance distributions

In contrast, the excess kurtosis values show notable variation. The photogrammetry–TLS comparison exhibits a relatively high excess kurtosis value (4.368), indicating a heavy-tailed distribution. As illustrated in Figure 7c, although the centre of the distribution appears close to a Gaussian shape, slight deviations

https://doi.org/10.5194/isprs-archives-XLIX-B2-2026-923-2026

can be observed in the tails, reflecting the occurrence of infrequent but significant extreme values. Meanwhile, the ULi–TLS and ULi–photogrammetry comparisons yield excess kurtosis values close to zero, suggesting distributions that are more consistent with normal behaviour.

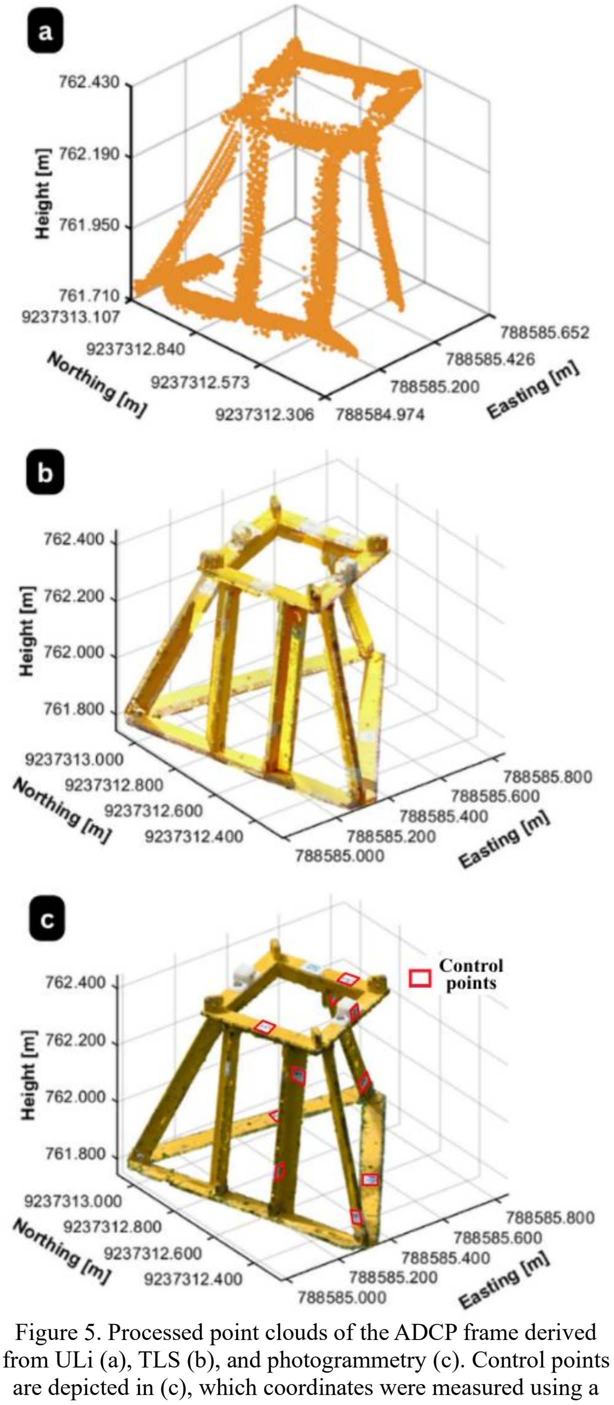

Figure 5. Processed point clouds of the ADCP frame derived from ULi (a), TLS (b), and photogrammetry (c). Control points are depicted in (c), which coordinates were measured using a total station from multiple benchmarks with known coordinates.

These results indicate that not all dataset comparisons follow a normal distribution, particularly the photogrammetry–TLS case. Therefore, error estimation based on parametric measures may not be appropriate. Instead, a robust approach using the median and MAD, as defined in Equation 3, is adopted because it is less sensitive to outliers.

Further outlier analysis based on the interquartile range (IQR) confirms the presence of outliers across all M3C2 distance datasets. The outliers are defined as values exceeding the upper bound *(Q3 + 1.5 × IQR)* or falling below the lower bound *(Q1 - 1.5 × IQR)*, where *Q1* and *Q3* represent the first (25th percentile) and third (75th percentile) quartiles, respectively (Walpole et al., 2011). As presented in Figure 8 and Table 4, the box-and-whisker plots clearly show the presence of outliers in each dataset.

Dataset Comparison	Number of outliers (points)	Number of outliers (%)
ULi–TLS	17,907	3.11
ULi–Photogrammetry	94,02	4.09
Photogrammetry–TLS	52,325	5.08

Table 4. Number and percentage of outliers identified in M3C2 distance using the IQR method for each dataset comparison

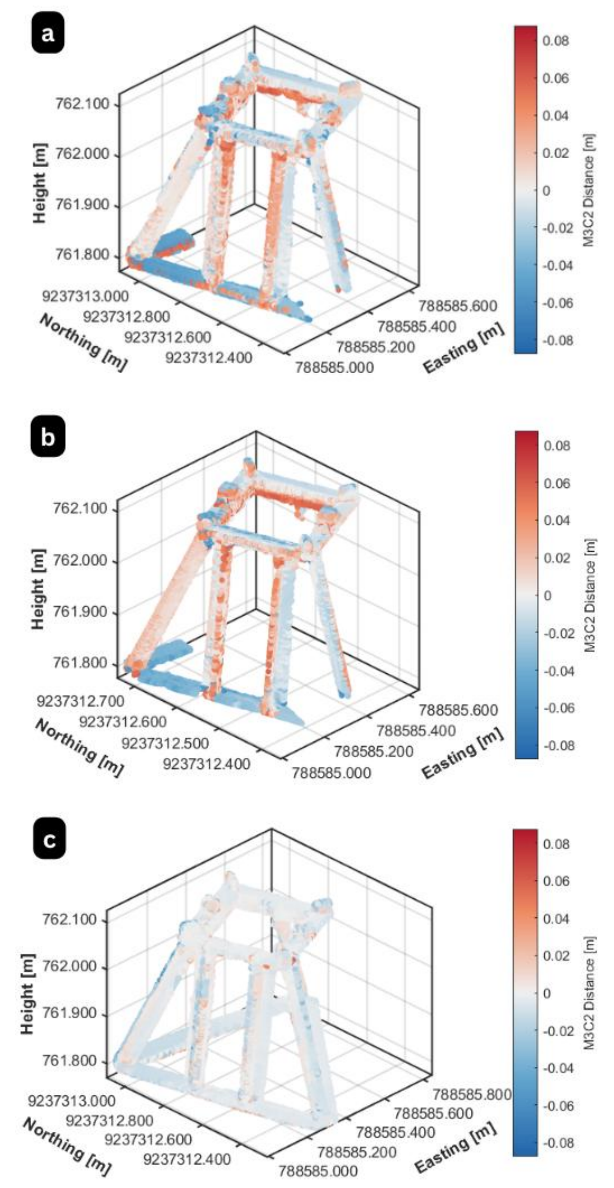

Figure 6. Visualisation of M3C2 distance results between ULi and TLS (a), ULi and photogrammetry (b), and photogrammetry and TLS (c).

These findings demonstrate that M3C2 distance data are affected by outliers and do not fully conform to a normal distribution, thereby reinforcing the use of median and MAD as robust measures for error assessment.

In comparisons involving ULi data, the lower point density limits the number of valid neighbourhoods where the M3C2 distances can be computed. Consequently, the number of detected outliers in ULi–TLS and ULi–photogrammetry comparisons appears lower, not necessarily due to better data quality, but rather due to the reduced number of valid comparison points. This is consistent with the smaller number of ULi points, as presented in Table 1.

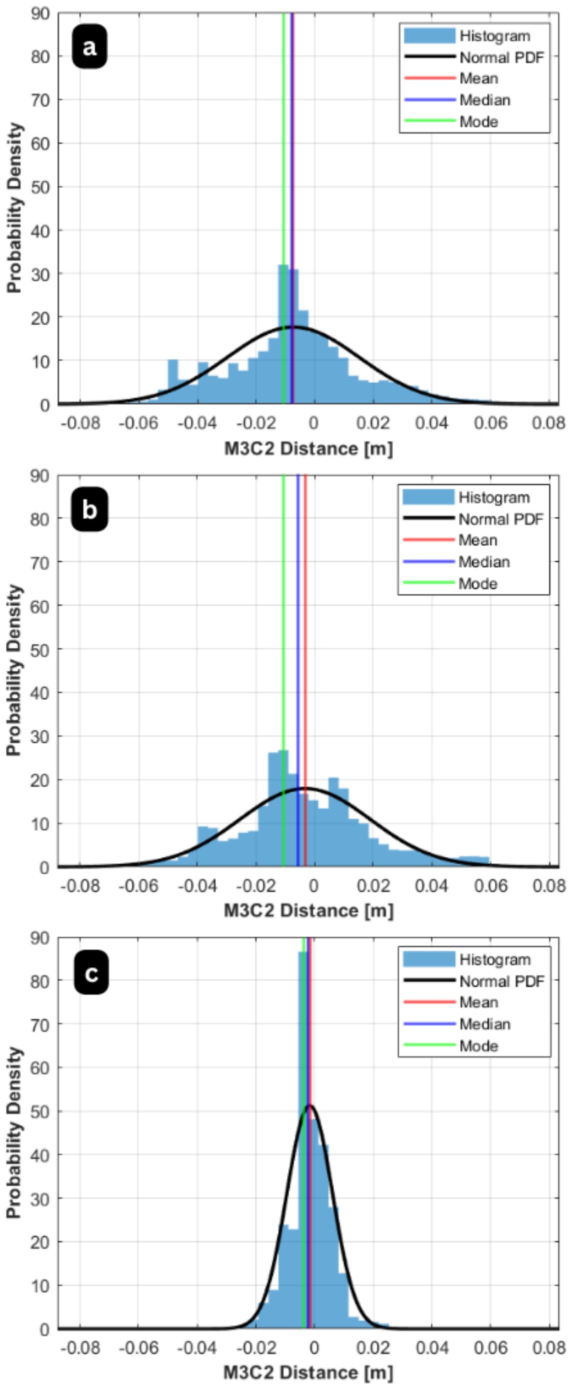

Figure 7. Histograms of M3C2 distance distributions with fitted normal probability density function (PDF) for dataset comparisons: TLS–ULi (a), ULi–photogrammetry (b), and photogrammetry–TLS (c).

3.3 Error measurement of underwater lidar

Based on the statistical parameters presented in Table 3 and calculated using Equation 3, the resulting deviations are summarised in Table 5.

The smallest M3C2 distance error is observed in the photogrammetry–TLS comparison, with a value of 0.002 ± 0.004 m. In comparisons involving ULi data, the ULi–photogrammetry pair shows a lower error (0.006 ± 0.013 m) compared to the ULi–TLS pair (0.008 ± 0.012 m), indicating that ULi measurements are slightly more consistent with photogrammetric data than with TLS.

Dataset Comparison	**Error (ε)**
ULi–TLS	0.008 ± 0.012 m
ULi–Photogrammetry	0.006 ± 0.013 m
Photogrammetry–TLS	0.002 ± 0.004 m

Table 5. Deviation derived from M3C2 distance distributions for each dataset comparison, expressed using the median and MAD

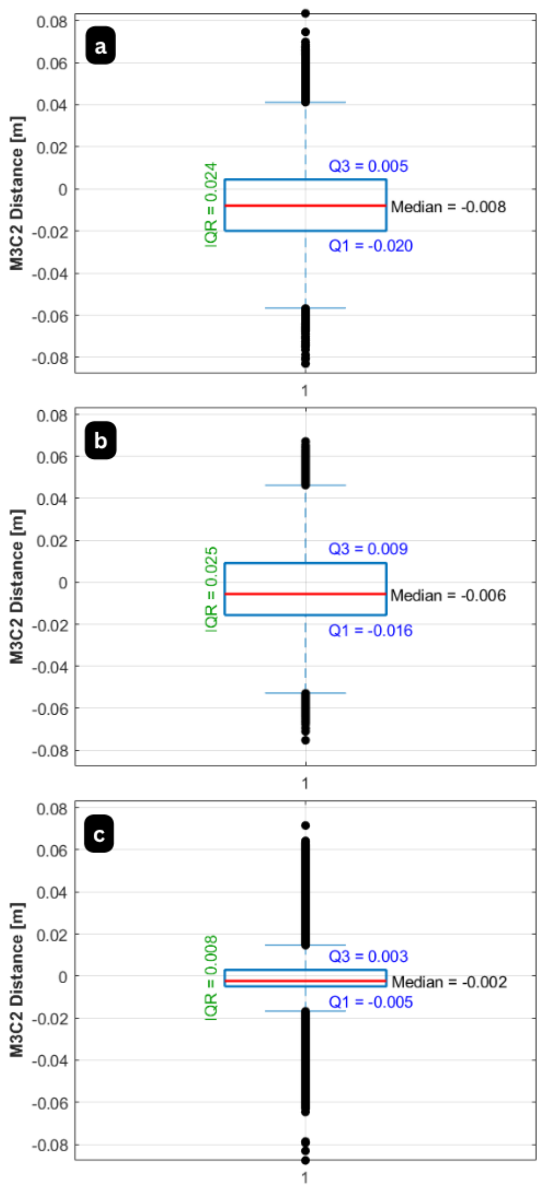

Figure 8. Box-and-whisker plots of M3C2 distance distributions: TLS–ULi (a), ULi–photogrammetry (b), and photogrammetry–TLS (c).

Overall, the median error values remain within the millimetre range, whereas the MAD values are notably larger, reaching the centimetre scale. This indicates that while the central tendency of the M3C2 distances suggests good geometric agreement, the dispersion of the data is influenced by the presence of outliers. Consequently, the geometric error of ULi relative to both TLS and photogrammetry can be considered to range from millimetre to centimetre levels.

3.4 Comparison of ADCP dimensions

Dimensional discrepancies among ULi, TLS, and photogrammetric measurements for each segment are presented in Figure 9. These discrepancies are expressed as pairwise differences between datasets, namely ΔTLS–ULi (ULi dimensions referenced to TLS), Δphotogrammetry–ULi (ULi dimensions referenced to photogrammetry), and ΔTLS–photogrammetry (photogrammetry dimensions referenced to TLS). The corresponding segments are illustrated in Figure 10 and were selected based on the completeness and availability of the ULi point cloud data.

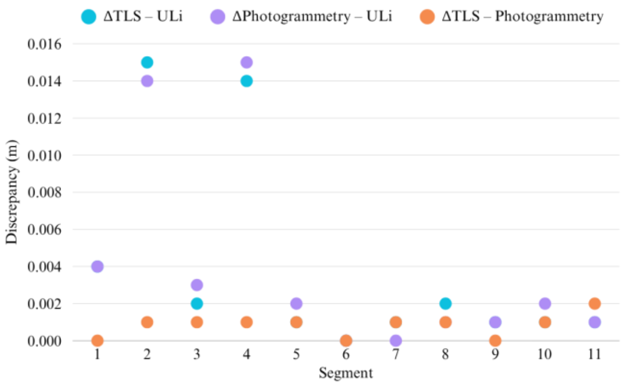

Figure 9. Absolute dimensional discrepancies between ULi, TLS, and photogrammetric measurements for each segment.

In general, the measurements exhibit differences generally within the centimetre to millimetre range. For segments 1–4, the ULi measurements are larger than those obtained from TLS and photogrammetry, with differences of approximately 0.002–0.015 m. In contrast, segments 5–7 exhibit very close agreement among all datasets, with differences typically below 0.002 m. Similarly, for segments 8–11, the measurements from all datasets are consistent, with differences generally within 0.001–0.002 m, as shown in Figure 9.

TLS and photogrammetric data acquisitions were conducted in land conditions, whereas the ULi data were acquired in shallow marine environments. This difference in acquisition conditions contributes to the observed discrepancies in the results, particularly for segments 2 and 4, where larger deviations were identified.

The performance of underwater lidar is strongly influenced by water turbidity, as signal penetration depth decreases with increasing turbidity (Saylam et al., 2017; Zimmerman et al., 2013) and the quality of the navigation solution. In this study, the shallow-water environment with low turbidity conditions was considered sufficiently suitable for data acquisition. Although only a single survey line was used, the ULi system was able to reconstruct the ADCP frame with dimensional differences generally within the centimetre to millimetre range when compared to TLS and photogrammetry results.

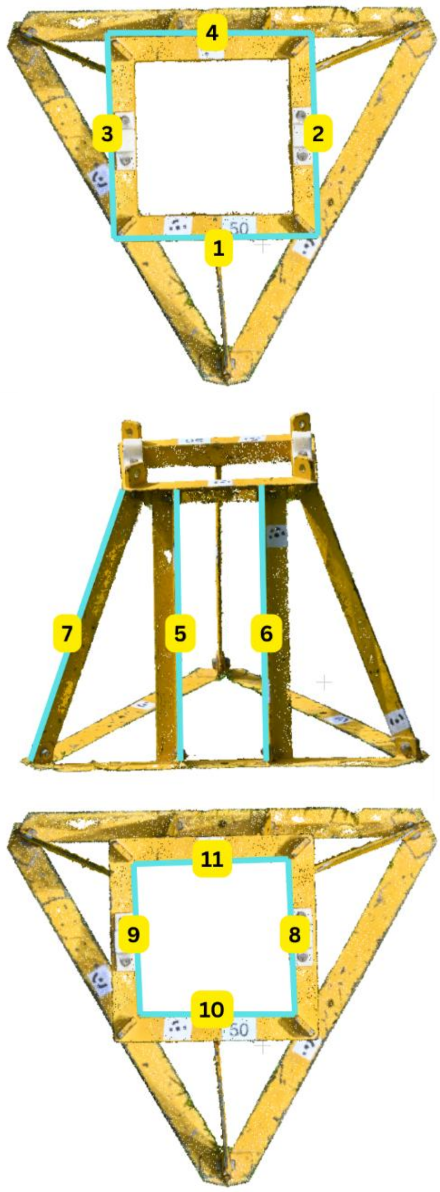

Figure 10. Locations of the 11 selected measurement segments on the ADCP frame used for dimensional comparison.

However, several factors inherent to underwater laser scanning may influence the accuracy of the ULi measurements. One important factor is the edge effect, where the finite size of the laser footprint causes partial reflections when the beam intersects object boundaries. In such cases, only part of the emitted energy is reflected from the target surface, while the remainder may be reflected from adjacent surfaces or lost, leading to measurement bias (Böhler & Marbs, 2005). During the segmentation process, outliers and reflections associated with edge effects were manually removed. Nevertheless, to further improve the results, the application of automated filtering methods could be considered to more effectively detect and eliminate such artefacts.

Another key factor is the difference in sensor distance to the object (Böhler & Marbs, 2005). The TLS and photogrammetric datasets were acquired at relatively close range, with an average sensor-to-object distance of approximately 2–3 m. In contrast, the ULi data were acquired at a greater distance of approximately 5–6 m. This increased range, combined with underwater attenuation effects, likely contributes to the slightly higher discrepancies observed in the ULi measurements.

4. Conclusion

This study presents a geometric accuracy assessment of point cloud data acquired using an ULi system, evaluated against reference datasets obtained from TLS and photogrammetry. The ULi data were collected in shallow water environments, whereas TLS and photogrammetric data were acquired on land.

Geometric discrepancies were quantified using the M3C2 distance, and error estimation was performed using robust statistical measures, the median and MAD. The results indicate that the error of ULi relative to TLS is 0.008 ± 0.012 m, while the error relative to photogrammetry is 0.006 ± 0.013 m. In comparison, the discrepancy between photogrammetry and TLS is significantly smaller, at 0.002 ± 0.004 m. Overall, the ULi achieves accuracy within the millimetre to centimetre range, although it does not reach the precision level of the terrestrial reference datasets.

Dimensional analysis of the ADCP frame further supports these findings. Larger discrepancies were observed in segments 2 and 4, with differences reaching the centimetre level, whereas the remaining segments had differences generally within the millimetre range. These variations are likely influenced by local factors, particularly in the upper parts of the ADCP frame, where edge effects may introduce additional uncertainties. The underwater environment also plays a role in the accuracy of ULi. Despite the ULi system being specifically designed for underwater operation, factors such as water properties and measurement range still affect the results.

In general, the ULi-derived point cloud demonstrates reliable performance in tropical shallow water with low turbidity, indicating its potential for underwater applications. However, further improvements, particularly in handling edge effects and optimising data processing, are recommended to enhance measurement accuracy.

Acknowledgements

The authors thank PT GPS Indosolution for supporting the TLS data acquisition, as well as all researchers and students involved in the collaborative project between HafenCity University (HCU) and ITB conducted from 19 to 28 September 2025. The authors especially thank Ellen Heffner and Annika L. Walter for acquiring the ULi data. The research conducted in this paper was also supported by the Digital Twins for Cultural Heritage (Twin4CH – https://twin4ch.github.io/) Junior Professorship Chair, financed by the French National Agency for Research (Agence nationale de la recherche – ANR).

References

Bobrowski, R., Winczek, M., Zięba-Kulawik, K., Wężyk, P., 2023. Best practices to use the iPad Pro LiDAR for some procedures of data acquisition in the urban forest. *Urban Forestry and Urban Greening*, *79*. doi.org/10.1016/j.ufug.2022.127815.

Böhler, W., Marbs, A., 2005. Investigating Laser Scanner Accuracy. *A Technical Report for Institute for Spatial Information and Surveying Technology*.

Chen, Q., Yam, J. W., Chua, S. Y., Guo, N., Wang, X., 2020. Characterizing the performance impacts of target surface on underwater pulse laser ranging system. *Journal of Quantitative Spectroscopy and Radiative Transfer*, *255*. doi.org/10.1016/j.jqsrt.2020.107267.

Fraunhofer Institute for Physical Measurement Techniques IPM, 2024. Underwater LiDAR System: Optical inspection of underwater infrastructure. In *Fraunhofer Institute for Physical Measurement Techniques IPM*.

Heffner, E., Walter, A. L., Scheider, A., Sternberg, H., 2025. Laboratory-based assessment of the Underwater Laser Scanner ULi. *International Archives of the Photogrammetry, Remote Sensing and Spatial Information Sciences*, *48*(2/W10-2025), 123–129. doi.org/10.5194/isprs-Archives-XLVIII-2-W10-2025-123-2025.

Hillman, S., Wallace, L., Reinke, K., Jones, S., 2021. A comparison between TLS and UAS LiDAR to represent eucalypt crown fuel characteristics. *ISPRS Journal of Photogrammetry and Remote Sensing*, *181*(April), 295–307. doi.org/10.1016/j.isprsjprs.2021.09.008.

Iacobucci, D., Román, S., Moon, S., Rouziès, D., 2025. A Tutorial on What to Do With Skewness, Kurtosis, and Outliers: New Insights to Help Scholars Conduct and Defend Their Research. *Psychology & Marketing*, *42*(5), 1398–1414. doi.org/https://doi.org/10.1002/mar.22187.

Kim, H, 2013. Statistical notes for clinical researchers : assessing normal distribution (2) using skewness and kurtosis. *Restorative Dentistry & Endodontics*, *38*(1), 52–54. doi.org/10.5395/rde.2013.38.1.52.

Koziel, S., Hilber, P., Westerlund, P., Shayesteh, E, 2021. Investments in data quality : Evaluating impacts of faulty data on asset management in power systems. *Applied Energy*, *281*(May 2020), 116057. doi.org/10.1016/j.apenergy.2020.116057.

Kraken Robotics, 2025. Kraken Subsea LiDAR: Advanced subsea LiDAR for rapid and precise measurements. In *Kraken Robotics*.

Lague, D., Brodu, N., Leroux, J., 2013. Accurate 3D comparison of complex topography with terrestrial laser scanner : Application to the Rangitikei canyon (N-Z). *ISPRS Journal of Photogrammetry and Remote Sensing*, *82*, 10–26. doi.org/10.1016/j.isprsjprs.2013.04.009

Li, S., Su, D., Yang, F., Zhang, H., Wang, X., Guo, Y., 2022. Bathymetric LiDAR and multibeam echo-sounding data registration methodology employing a point cloud model. *Applied Ocean Research*, *123*(2021), 103147. doi.org/10.1016/j.apor.2022.103147.

Rashdi, R., Garrido, I., Balado, J., Del Río-Barral, P., Rodríguez-Somoza, J. L., Martínez-Sánchez, J., 2024. Comparative Evaluation of LiDAR systems for transport infrastructure: case studies and performance analysis. *European Journal of Remote Sensing*, *57*(1). doi.org/10.1080/22797254.2024.2316304.

Rho, S., Joe, H., Sung, M., Kim, J., Kim, S., Yu, S., 2025. Multi-Sonar Fusion-based Precision Underwater 3D Reconstruction for Optimal Scan Path Planning of AUV. *IEEE Access*, *13*, 35157–35173. doi.org/10.1109/ACCESS.2025.3542084.

Saylam, K., Brown, R. A., Hupp, J. R., 2017. Assessment of depth and turbidity with airborne Lidar bathymetry and multiband satellite imagery in shallow water bodies of the

Alaskan North Slope. *International Journal of Applied Earth Observation and Geoinformation*, *58*, 191–200. doi.org/10.1016/j.jag.2017.02.012

Sørensen, F. F., Mai, C., Benzon, M. Von, Liniger, J., Pedersen, S., 2025. The localization problem for underwater vehicles : An overview of operational solutions. *Ocean Engineering*, *330*. doi.org/10.1016/j.oceaneng.2025.121173

Toschi, I., Rodríguez-Gonzálvez, P., Remondino, F., Minto, S., Orlandini, S., Fuller, A., 2015. Accuracy evaluation of a mobile mapping system with advanced statistical methods. *International Archives of the Photogrammetry, Remote Sensing and Spatial Information Sciences - ISPRS Archives*, *40*(5W4), 245–253. doi.org/10.5194/isprsarchives-XL-5-W4-245-2015

Voyis, 2021. Data Sheet and Product Information: Insight Underwater Laser Scanners. In *Voyis Imaging Incorporated*.

Walpole, R. E., Myers, R. H., Myers, S. L., Ye, K. E., 2011. *Probability and Statistics for Engineers and Scientists* (D. Lynch (ed.); 9th ed.). Pearson Education.

Walter, A. L., Heffner, E., Scheider, A., Sternberg, H., 2025. Underwater laser scanning: Evaluating the performance of ULi in laboratory and real-world environments to determine the achievable level-of-detail. *The International Hydrographic Review*, *31*(1), 152–164. doi.org/10.58440/ihr-31-1-n05

Werner, C. S., Gangelhoff, J., Frey, S., Steiger, D., Reiterer, A., 2023. Development of a compact pulsed time-of-flight LiDAR platform for underwater measurements. *The International Hydrographic Review*, *29*(2), 200–207. doi.org/10.58440/ihr-29-2-n09

Yang, M., Hu, J., Li, C., 2019. *An In-Depth Survey of Underwater Image Enhancement and Restoration*. *7*. doi.org/10.1109/ACCESS.2019.2932611

Zimmerman, R. C., Sukenik, C. I., Hill, V. J., 2013. Subsea LIDAR systems. In J. Watson , O. Zielinski (Eds.), *Subsea Optics and Imaging*. Woodhead Publishing. doi.org/10.1533/9780857093523.3.471